Effective Production of Poly(3-alkylthiophene) Nanofibers by means of Whisker Method using Anisole Solvent: Structural, Optical, and Electrical Properties

Sadaki Samitsu,*,†,‡ Takeshi Shimomura,§,† Seiji Heike,|| Tomihiro Hashizume,||,⊥,# and Kohzo Ito*,†

Department of Advanced Materials Science, Graduate School of Frontier Sciences, The University of Tokyo, 5-1-5-603 Kashiwanoha, Kashiwa, Chiba 277-8561, Japan, Advanced Research Laboratory, Hitachi, Ltd., Hatoyama 350-0395, Japan, Department of Physics, Tokyo Institute of Technology, Meguro 152-8550, Japan, and WPI Advanced Institute for Materials Research, Tohoku University, Sendai 980-8577, Japan

Received May 21, 2008; Revised Manuscript Received August 8, 2008

ABSTRACT: The whisker method using anisole solvent was developed for effective production of high-aspect-ratio poly (3-alkylthiophene) (P3AT) nanofibers, and alkyl chain length dependence on nanofiber formation and their properties were fully investigated. The nanofibers have an anisotropic cross section of 3−4 nm height and 24−27 nm width, which slightly increase with the alkyl chain length, and the aspect ratio reaches 100−1000. The nanofibers consist of more than 10^4 parallel stacks of the extended polymer backbones along the nanofiber long axis and of 2−3 laminated layers of the polymer backbones separated by alkyl side chains. The nanofiber formation originates from quasi-one-dimensional crystallization of P3ATs induced by both an attractive $\pi-\pi^*$ interaction between polymer backbones and the crystallization of alkyl side chains. Carrier transport properties of a $AuCl_3$-doped nanofiber network and single nanofibers, both of which are explained by a quasi-one-dimensional variable-range hopping (VRH) model irrespective of alkyl chain length, indicate that the origin of the random potential that localizes the carriers should be attributed not to the bridges between nanofibers but to some factor involved in a single nanofiber.

Introduction

Conducting polymer nanofibers have received much attention in scientific research and industrial applications of organic electronics because their intrinsic one-dimensionality provides excellent carrier transport.[1,2] Polythiophene derivatives including poly (3-alkylthiophenes) (P3ATs) are one of the most promising conducting polymers[3] because, in addition to good environmental stability, the large overlap between the π orbitals delocalized over the polymer chains and well-ordered semicrystalline structure result in high carrier transport.[4−6] While unsubstituted polythiophene is insoluble and infusible, the alkyl side chains of P3ATs render them highly soluble in common organic solvents[7,8] and hence suitable for applications to solution-based nanofiber production. Conducting polymer nanofibers of polythiophene derivatives have been produced by various solution-based procedures: template method,[9] electrospinning,[10] nontemplate method,[11] Langmuir−Blodget method,[12] dip-pen nanolithography,[13] copolymerization,[14] molecular combing,[15] self-organization on a substrate during drying,[16,17] and self-organized whisker formation in a solution.[18−21] The whisker method should have potential advantages from an industry viewpoint due to low-cost and mass production of nanofibers. Unfortunately, however, it has not been extensively studied, and more investigations are required for achieving conclusive understanding of the physical mechanism of nanofiber formation and establishing a standard process of fabricating nanofiber devices. In particular, the effect of the alkyl chain length on nanofiber formation and carrier transport should be of interest because many studies on bulk and thin films of P3ATs have revealed that the alkyl chain length has large influence on many physical properties of P3ATs: solubility,[22] melting point,[23,24] crystalline structure,[25] optical property,[8,26] and carrier transport property.[27] Although we have preliminarily investigated the nanofiber production of solvent-soluble conducting polymers by using the whisker method,[19] the poor reproducibility of the nanofibers caused difficulties in the systematic investigation of their morphological and electrical properties. In this article, we report the effective production of P3AT nanofibers by means of the whisker method using anisole solvent. The reliable method has provided an opportunity to elucidate the dependence of the formation mechanism and the morphological, optical, and electrical properties of the nanofibers on the alkyl chain length by using atomic force microscopy (AFM), UV−vis absorption spectroscopy, X-ray diffraction (XRD) measurements, and conductivity measurements. We reveal that the nanofiber formation results from quasi-one-dimensional crystallization of P3ATs and discuss the carrier transport in a nanofiber network and single nanofibers by comparing their four-probe conductivities measured using 36-μm-spacing electrodes with those of 250-nm-spacing ones.

* Corresponding authors. E-mail: ssamitsu@scphys.kyoto-u.ac.jp (S.S.); kohzo@k.u-tokyo.ac.jp (K.I.).
† Department of Advanced Materials Science, Graduate School of Frontier Sciences, The University of Tokyo.
‡ Present address: Department of Physics 1, Faculty of Science, Kyoto University, Kyoto 606-8502, Japan,
§ Present address: Graduate School of Bio-Applications and System Engineering, Tokyo University of Agriculture and Technology, Koganeishi, Tokyo 184-8588, Japan
|| Advanced Research Laboratory, Hitachi, Ltd.
⊥ Department of Physics, Tokyo Institute of Technology.
WPI Advanced Institute for Materials Research.

Experimental Section

Materials. Regioregular poly(3-butylthiophene-2,5-diyl; P3BT), poly(3-hexylthiophene-2,5-diyl; P3HT), poly(3-octylthiophene-2,5-diyl; P3OT), poly(3-decylthiophene-2,5-diyl; P3DT), regiorandom poly(3-hexylthiophene-2,5-diyl; RRa-P3HT), anhydrous anisole (99.7%), anhydrous chloroform (>99.7%, including amylene as a stabilizer), anhydrous hexane (95%), anhydrous acetonitrile (99.8%), octadecyltrichlorosilane (OTS) (>90%), and gold(III) chloride

10.1021/ma801128v CCC: $40.75
Published on Web 10/11/2008

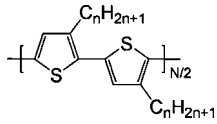

Figure 1. Chemical structure of regioregular P3ATs: P3BT, $n = 4$; P3HT, $n = 6$; P3OT, $n = 8$; and P3DT, $n = 10$.

Table 1. Molecular Weights of As-Received (Aldrich) and Soxhlet-Extracted P3ATs (Acetone, Hexane, CH_2Cl_2, THF, and $CHCl_3$ Fractions)[a]

		Aldrich	acetone	hexane	CH_2Cl_2	THF	$CHCl_3$
P3BT	wt %		3.9	11.8	11.2	23.1	49.9
	M_n	10500		3700	6100	8200	11700
	M_w	20400		4000	7900	12800	21500
	M_w/M_n	1.94		1.09	1.28	1.56	1.84
	N	76		27	44	59	85
P3HT	wt %		2.6	1.7	12.2	83.6	
	M_n	17500		4300	9900	27400	
	M_w	44900		5000	15000	110000	
	M_w/M_n	2.57		1.17	1.51	4.00	
	N	105		26	60	165	
P3OT	wt %		4.2	7.8	56.8	31.2	
	M_n	7600		7300	18000	38400	
	M_w	33900		9100	30500	72700	
	M_w/M_n	4.44		1.24	1.69	1.89	
	N	39		38	93	198	
P3DT	wt %		3.0	6.5	78.6	11.9	
	M_n	30500		8900	32800	46500	
	M_w	104000		12900	85800	181200	
	M_w/M_n	3.40		1.45	2.62	3.89	
	N	137		40	148	209	

[a] Abbreviations: THF, tetrahydrofuran; wt %, weight percentage of Soxhlet-extracted P3AT fractions; M_n, number-averaged molecular weight; M_w, weight-averaged molecular weight; N, number of thiophene units calculated from the corresponding M_n values. The M_n and M_w values were determined by the SEC measurements in terms of a polystyrene-equivalent molecular weight.

($AuCl_3$) (99.99%) were purchased from Aldrich (Milwaukee, WI). Other chemicals were purchased from Wako Pure Chemical Industries, Ltd. (Osaka, Japan). The chemical structure of the regioregular P3ATs is shown in Figure 1. On the basis of the information provided by the supplier, in contrast to the RRa-P3HT containing equivalent number of head-to-tail and head-to-head (and tail-to-tail) linkages, the regioregular P3ATs predominantly consist of head-to-tail linkages: 97% for P3BT and more than 98.5% for other P3ATs used. A silicon wafer with a 150-nm-thick thermally grown SiO_2 layer on its top surface (SiO_2/Si) was purchased from NTT Advanced technology (Tokyo, Japan). The dependence of the nanofiber formation on the molecular weight of P3AT was investigated by using the P3ATs that were Soxhlet extracted with alternative solvent exchange of acetone, hexane, dichloromethane, tetrahydrofuran (THF), and chloroform. The molecular weights of the as-received and the Soxhlet-extracted P3ATs are listed in Table 1. Some of the highest-molecular-weight fractions of the extracted P3ATs exhibited the M_n/M_w value slightly larger than that of as-received ones. Soxhlet-extraction at high temperatures (ca. 60 °C) may cause unexpected polymerization of P3ATs.

SEC Characterization of P3AT. Size-exclusion chromatography (SEC) measurements were performed on a Shimadzu high-performance liquid chromatography system equipped with a photodiode array UV−vis detector. A P3AT solution (0.10 wt % in chloroform) was passed through a 0.20-μm polytetrafluoroethylene (PTFE) filter and injected into a SEC system of three chromatography columns: a Shodex K-800D guard column, a Shodex K-803 L column (diameter, 8.0 mm; length, 300 mm; pore size, 6 μm), and a Shodex K-804 L column (diameter, 8.0 mm; length, 300 mm; pore size, 7 μm). Chloroform containing a stabilizer (0.5% ethanol) was used as the eluent (40 °C, 1.0 mL/min). The SEC system was calibrated with polystyrene standards (PS-oligomer kit, Tosoh Co., Ltd., Tokyo, Japan) and gave the molecular weight of a P3AT in terms of a polystyrene-equivalent molecular weight.

Preparation of a Nanofiber Solution. In a typical procedure, a P3AT (1.0 mg) was added to anisole (2.0 g) in a 5-mL glass vial equipped with fluorinated silicone packing, and the solution was stirred with heating (>70 °C). P3HT, P3OT, and P3DT readily dissolved in the anisole. On the other hand, P3BT dissolved only partially due to its shorter alkyl side chains. The P3BT solution was further stirred at 70 °C overnight and the residue was removed by filtration through a 0.45-μm PTFE filter above 70 °C; the filtrate was used on further investigation. Although the concentration of the P3BT solution decreased slightly on removing the residue, it is described by the weight percent of the polymer initially added to the solution, for simplicity. After the stirring was stopped at 70 °C, the P3AT solutions were gradually cooled to 20 °C in a rate-controllable liquid circulator bath (Haake Phoenix II P1-C25P, Thermo Electron Corp.) at a constant cooling rate of 25 °C/h. On rapid cooling, the P3AT solutions that had been heated above 70 °C were quickly cooled to the room temperature within 15 min by holding the glass vial at the room temperature; although the cooling rate was not regulated at a constant value, it was much faster than 25 °C/h. Nanofibers mainly grow in the solution during cooling of temperatures. These nanofiber solutions were used within several days after preparation. In some experiments, anisole containing 20-vol. % chloroform was used as a solvent.

Characterization of P3AT Nanofibers. A P3AT nanofiber solution was spin coated at 3000 rpm on a SiO_2/Si substrate and the residual solvents were removed by vacuum-drying. Spin coating was performed in air using a commercial spin coater (ACT-300D, ACTIVE Co., Ltd., Saitama, Japan). The P3AT nanofibers thus deposited on the substrate were imaged in air by using a MultiMode AFM Nanoscope IIIa (Veeco Instruments Inc.) operated in the tapping mode. Typical AFM imaging was performed using a silicon cantilever having a spring constant of 40 N/m and a resonant frequency of 300 kHz (MPP-11100, Veeco Instruments Inc.). We carefully adjusted the amplitude (setpoint) of the cantilever to obtain a clear image of nanofibers. The coverage density of nanofibers was determined from the analysis of their area in a 5-μm scan image by using the Nanoscope software. Three key factors were considered for careful determination of the nanofiber dimensions using AFM imaging: (1) degree of dispersion of nanofibers on a flat substrate, (2) a small scan size that provides sufficient resolution, (3) the effect of AFM tip geometry. As mentioned in later, the spin coating of a dilute nanofiber solution (0.010 wt %) deposits well-dispersed nanofibers on a flat SiO_2/Si substrate whose roughness was much smaller than their height. Smaller scan sizes of AFM images (1×1 μm; 512×512 pixels) offer sufficient resolution to determine the nanofiber dimensions. Previous studies have revealed that the geometry and properties of an AFM tip have serious influence on the AFM images of a small object that is nearly the same as the tip radius of curvature.[28] In order to check the effect of a tip, two cantilevers having different tips were used in AFM imaging for determination of height and width distribution: a Si tip and a carbon-whisker (CW) tip (NSC05, NT-MDT Co.). The spring constant of the CW-tip cantilever was 14 N/m and the resonant frequency was 320 kHz. The CW tip has a steeper geometry than the Si tip.[29] The height and width of a nanofiber were determined from the cross sectional AFM images obtained perpendicular to the long axis of the nanofiber. The width of the nanofiber is defined as full width at half-maximum (fwhm) of the cross section. Optical-microscope images were recorded on an Olympus BX-51 M metallurgical microscope using reflected light illumination equipped with a CCD camera (DP21, Olympus Corp.).

UV−vis absorption spectra were recorded on a Shimadzu UV-3150 spectrometer equipped with a temperature controller unit using a liquid circulator. A P3AT solution was filled in a 2-mm-thick quartz cell sealed with a PTFE cap. For UV−vis measurements, nanofiber thin films of P3ATs were drop cast from the respective nanofiber solutions (0.050 wt %) on OTS-modified quartz substrates.

XRD measurements were performed using a Rigaku diffractometer (Type 4037) with graded d-space elliptical side-by-side multilayer optics. P3AT nanofibers were collected by drying in vacuo using a 0.050-wt % nanofiber solution or precipitation from

methanol using a 0.10-wt % nanofiber solution. Monochromated Cu Kα radiation ($\lambda = 1.542$ Å), generated at 40 kV and 30 mA, irradiated the nanofibers placed into a quartz capillary (diameter, 1.5 mm; wall thickness, 0.01 mm) or between Mylar films (Teijin DuPont Films Japan Limited, Tokyo, Japan). XRD patterns were recorded on a Rigaku R-AXIS IV imaging-plate detector. The camera length was 150 mm. Since randomly oriented nanofibers showed a ring-like diffraction pattern, the diffraction pattern was converted into 2θ-intensity profiles using the Rigaku R-AXIS software. The 2θ-intensity profiles were corrected by subtracting the background intensity of the quartz capillary or the Mylar film. The diffraction peak at $2\theta_B$ in the 2θ-intensity profile was fitted by a Gaussian function, which gave the fwhm $\Delta\theta$ of the peak. The size of the coherent domains (crystallites) ξ was roughly estimated from the Scherrer equation given by eq 1[30]

$$\xi = \frac{0.9\lambda}{(\Delta\theta)\cos\theta_B} \quad (1)$$

Conductivity Measurements of a Nanofiber Network and Single Nanofibers. Substrates suitable for the conductivity measurements of a nanofiber network were made by fabricating platinum electrodes on SiO_2/Si substrates using conventional photolithography. From their optical-microscope images, typical spacing and width of the electrodes, L_{long} and W_{long}, were found to be 36 and 500 μm, respectively. On the other hand, substrates suitable for the conductivity measurements of single nanofibers were made by fabricating platinum electrodes on SiO_2/Si substrates using photolithography in combination with AFM lithography according to the fabrication method reported by Kato et al.[31] From their AFM images, typical spacing and width of the four-probe electrodes, L_{short} and W_{short}, were found to be 250 nm and 9 μm, respectively. Typical thickness and roughness of the platinum electrode were respectively about 10 and 1 nm. The substrates with electrodes were cleaned in a piranha solution (H_2SO_4: 30-wt % H_2O_2 = 3:1 v/v) for 15 min at 45 °C. (***Caution! Piranha solution reacts violently with organic materials.***) An OTS solution (10 mmol/L in anhydrous hexane) was freshly prepared and passed through a 0.20-μm PTFE filter. The substrate surface was modified by dipping it in the OTS solution for 10 min, followed by three times washing with chloroform under argon atmosphere. Prior to the spin coating of nanofibers, the current between electrodes was measured in order to check their electrical isolation. The electrodes that showed a current less than 0.2 pA were selected and used for the subsequent electrical measurements. A P3AT nanofiber solution in a solvent mixture of anisole/chloroform (4:1, vol. %) was spin coated on the substrate at 500 rpm for 10 s and 1500 rpm for 120 s, leading to the deposition of the P3AT nanofibers between the electrodes. The concentration of the solution was 0.050 wt % and 0.010 wt % for depositing a nanofiber network and single nanofibers between the electrodes, respectively. In order to avoid an electrical leakage through the substrate edges, the nanofibers placed near the edges were wiped off by using a cotton swab soaked with *p*-xylene. Further, so as to avoid the unintentional doping of the solution by the atmospheric oxygen, it was sealed with argon gas during nanofiber formation and its exposure to air during spin coating was kept to the minimum (<10 min). $AuCl_3$ was used as an acceptor dopant in P3AT nanofibers. In the absence of a P3AT nanofiber, the current between the electrodes dipped in the $AuCl_3$ solution was comparable to the background current, indicating that $AuCl_3$ does not cause a serious leakage current.

A conductivity measurement setup consists of a probe station chamber (ARK-LIPS-LV-2, Nagase Electronic Equipment Service Co., Ltd.) equipped with a Keithley source-measure unit (Model 236), and two Keithley electrometers (Model 6514). The nanofibers deposited between electrodes were introduced in the chamber, and subsequently the pressure in the chamber was reduced below 10^{-5} Torr using a turbomolecular pump. Sample temperatures were controlled in the range of 20−300 K by using a cryogenic refrigerator and a heating block. In darkness, the conductivity of the nanofibers was measured using two- and four-probe methods.

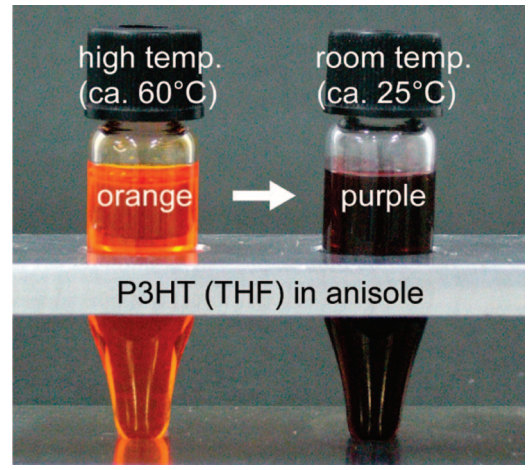

Figure 2. Photograph of a 0.050-wt % P3HT solution in anisole: (left) at a high temperature (ca. 60 °C) and (right) at room temperature (ca. 25 °C). P3HT Soxhlet-extracted from THF was used.

In the two-probe configuration, current voltage ($I-V$) characteristics were recorded using the source-measure unit. In the four-probe configuration, a potential difference was applied across the two outer electrodes by using the source-measure unit, and the current I_0 flowing between them and the voltages V_1 and V_2 of the two inner electrodes with respect to the ground were independently recorded using the source-measure unit and the two electrometers. The voltage drop V_{12} between the inner electrodes was calculated by subtracting V_2 from V_1. The two- and four-probe conductances of the nanofibers, G_{two} and G_{four}, were respectively determined from the slopes of the $I-V$ and I_0-V_{12} characteristics in their respective Ohmic regions. The thickness of a nanofiber network t was assumed to be the same as the average height of the respective P3AT nanofiber h_{av} because typical cross section of a pit in an AFM image exhibited a step height comparable to the h_{av}. The effective width of 36-μm-spacing electrodes W^{ef}_{long} was assumed to be proportional to the surface coverage of nanofiber ϕ between the electrodes. The effective width of 250-nm-spacing electrodes W^{ef}_{short} was calculated from the number of the nanofibers bridging the inner electrodes, N, and the average width of the nanofiber w_{av}. The h_{av} and w_{av} were respectively determined to be 3−4 nm and 24−27 nm from the following AFM measurement. As a result, the four-probe conductivity of nanofiber σ was calculated from eq 2

$$\sigma = G_{four}\frac{L}{W^{ef}_{\alpha}t} \quad (2)$$

,

$$W^{ef}_{long} = W\times\phi \quad \text{(36-}\mu\text{m-spacing electrodes)}$$

$$W^{ef}_{short} = N\times w_{av} \quad \text{(250-nm-spacing electrodes)}$$

where α is long or short.

Assuming that the four-probe resistance represents the intrinsic resistance of the nanofiber networks and the two-probe one represents the series equivalent of the resistance of the nanofiber networks and two contact resistances, the contact resistance per unit width of the electrodes R_c was calculated from eq 3

$$R_C = \frac{1}{2}\left(\frac{1}{G_{two}} - \frac{1}{G_{four}}\right)\times W^{ef}_{long} \quad (3)$$

Results and Discussion

Nanofiber Production. The dissolution of P3AT in anisole produced a transparent orange solution at high temperatures (>70 °C). During cooling, the solutions of all the P3ATs displayed a dramatic color change; P3BT and other P3AT solutions respectively turned brown and purple at 20 °C (shown in Figure 2). AFM images showed one-dimensional nanofibrillar

structures on SiO_2/Si substrates where the solutions were spin coated. The P3AT nanofibers had the height of a few nanometers and the length of several micrometers, which represent their high aspect ratio and will be discussed in detail later. It is important to note that the use of anisole solvent yielded high-aspect-ratio nanofibers of all the P3ATs investigated here, although the whisker method using other solvents such as *p*-xylene, cyclohexanone, and toluene has been reported to produce nanofibers of only one or two P3ATs.[18−20] In contrast to the P3HT nanofiber in cyclohexanone that precipitated within a few days at room temperature,[19] the nanofibers of all the P3ATs produced in this study were stably dispersed in anisole over a week without macroscopic precipitation.

We investigated the effects of production parameters on the nanofiber formation in anisole: (1) cooling rate, (2) the concentration of P3AT, and (3) polymer regioregularity. In this study, P3AT nanofibers were obtained by rapid cooling and also by gradual cooling (25 °C/h), in contrast to the P3HT nanofiber in *p*-xylene that were reported to be produced only by gradual cooling.[18−20] The rapid cooling often resulted in a shorter length of the nanofibers than the gradual cooling. The short nanofiber length of the order of 100 nm is similar to that of the P3HT nanofiber produced by solvent-nonsolvent method.[21] Nonetheless, the cooling rate did not crucially influence the production of P3AT nanofibers in anisole in the range investigated. The dependence of nanofiber formation on the concentration of P3AT in anisole was investigated by gradual cooling. P3HT nanofibers were obtained for a wide concentration range of 0.005−0.5 wt %. A solution having a P3HT concentration higher than 1.0−2.0 wt % finally gelled at room temperature. Thermoreversible gelation of P3AT/xylene systems has been reported and investigated in detail by Malik et al.,[32] and a fibrillar network structure was found in dried gels by using scanning electron microscopy. Similarly, the gel of a P3AT/anisole system may consist of a three-dimensional nanofibrillar network because the high-aspect-ratio nanofibers produced in a concentrated solution readily form physical cross-links in the gel. The low-concentration limit to obtain a P3HT nanofiber in anisole is at least 1 order of magnitude lower than that in *p*-xylene.[19] The alkyl chain length of P3ATs had little influence on the concentration range of their solutions that yielded nanofibers. The wide ranges of P3AT concentrations and cooling rates employed in this study enabled us to reproducibly and reliably obtain P3AT nanofibers. In contrast to the cooling rate and the P3AT concentration, polymer regioregularity can still be a crucial parameter dominating nanofiber formation; the regioregular P3ATs yielded nanofibers, but RRa-P3HT did not. The disturbed chain regularity of RRa-P3HT could disturb the self-organization of the polymer chains into a well-ordered lamellar structure.[33] This result is consistent with the explanation that the nanofiber formation of P3ATs in a solution is dominated by the crystallization of their polymer chains, which was previously proposed for the whisker formation of P3HT[17−20,24] and other regioregular conducting polymers.[19] Furthermore, the following UV−vis absorption and XRD measurements support the crystallization of P3ATs into the nanofibers.

The abovementioned results reveal that the selection of a solvent is one of the most influential factors governing nanofiber formation and that anisole is more appropriate than other solvents used in previous studies.[18−21] A possible scenario of nanofiber formation is as follows; P3ATs are isolated at a higher temperature due to dissolution and gradually self-assemble into nanofibers at a lower temperature due to low saturating concentration. A rough measure of polymer solubility is provided by the difference between the solubility parameter δ of the polymer and that of the solvent: the polymer can be soluble if this difference is small; insoluble, otherwise. Neher and co-workers have determined δs of P3HT and P3OT at room temperature to be 9.1 and 8.9 $cal^{1/2}\ cm^{-3/2}$, respectively, by means of solvent-nonsolvent titration.[34] δ of *p*-xylene (8.8 $cal^{1/2}\ cm^{-3/2}$ [35]) is modestly different from that of P3HT but sufficiently close to that of P3OT; therefore, the consequent low solubility of P3HT in *p*-xylene resulted in the formation of P3HT nanofibers, whereas the high solubility of P3OT prevented the formation of P3OT nanofibers. The differences between δ of cyclohexanone (9.9 $cal^{1/2}\ cm^{-3/2}$ [35]) and those of P3HT and P3OT were so large that they could result in macroscopic precipitates due to poor solubility, which prevents the formation of high-aspect-ratio nanofibers. On the other hand, δ of anisole (9.5 $cal^{1/2}\ cm^{-3/2}$ [35]) is modestly different from those of both P3HT and P3OT; therefore, the consequent higher solubility at high temperatures and lower solubility at room temperature can induce their self-assembly into nanofibers at near room temperature. However, the effect of a solvent on nanofiber formation is not exactly understood at present; in particular, its temperature dependence, which should be an important factor for nanofiber formation. Further investigation is necessary for achieving a complete understanding of the effect of solvent properties on nanofiber formation.

AFM Measurement. P3AT nanofibers produced in anisole were spin coated on SiO_2/Si substrates and their morphology was characterized using AFM. Although AFM images showed that the nanofibers had a one-dimensional nanofibrillar structure, some of the images included the nanofiber aggregates consisting of several tens of nanofibers, which were heterogeneously distributed on the substrate. In order to suppress the aggregation of nanofibers in a solution, we used a solvent mixture of anisole containing 20 vol. % of chloroform because chloroform is a moderately good solvent for P3ATs.[36] A P3AT solution in the solvent mixture of anisole/chloroform was gradually cooled to 20 °C and further stored at 20 °C for 12 h, followed by spin coating on a SiO_2/Si substrate. The spin coating of a 0.050-wt % solution gave uniformly distributed nanofibers, leading to dense network morphology (shown in left images of Figure 3). The surface coverage of the nanofiber network was determined to be 30%−60%. In contrast to the dense nanofiber network, well-dispersed nanofibers were obtained by the spin coating of a 0.010-wt % solution (shown in right images of Figure 3). Their surface coverage was determined to be 10%−25%. The concentration of the nanofiber solution roughly dominates the surface coverage of the nanofibers.

The height and width of a nanofiber were determined from magnified AFM images (1 × 1 μm scan size). Typical AFM images and their cross sections are shown in Figure 4. For all P3ATs, the height distributions of nanofibers exhibited two peaks: one peak in the 2−4-nm range and the other peak in the 4−6-nm range; mostly, the former is sharper and has a higher frequency than the latter (see the Supporting Information). The height measurements were performed on those nanofiber sections that did not overlap with any other nanofiber, which excludes the possibility that the 4−6 nm peak might have resulted from the overlap of nanofibers. Therefore, a stepwise increment in the height of nanofiber, which increases with the alkyl chain length, indicates layer growth of the nanofibers in the height direction. Average height h_{av} and its standard deviations σ_h are listed in Table 2. The h_{av} shifted to higher values with an increase in the alkyl chain length. For the same alkyl chain length, the h_{av} determined using the CW tip was a factor of 1.1−1.4 larger than that determined using the Si tip. This is probably due to lower loading force of the CW tip than the Si tip.[37] The width distributions of the nanofibers of all P3ATs exhibited a symmetrical peak at 25−30 nm, and therefore, the histograms were fitted by a single Gaussian curve (see Supporting Information). The peak positions w_{av} and their

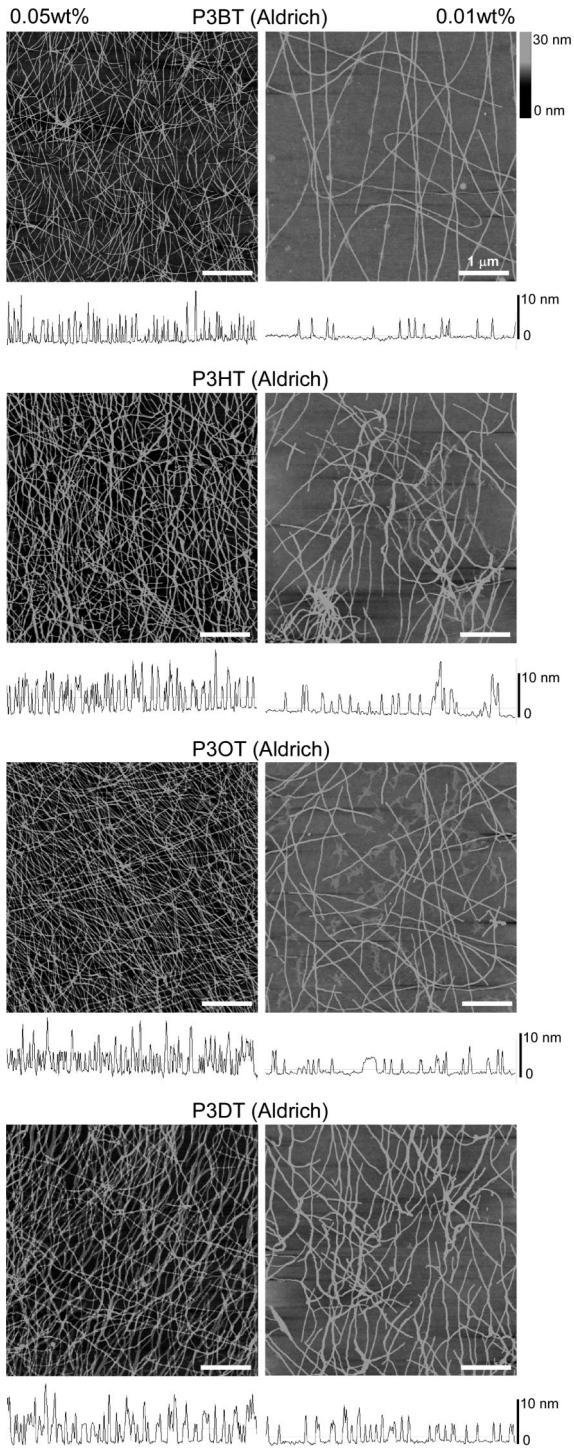

Figure 3. AFM images (upper) and their typical cross sections (lower) of P3AT nanofibers. The nanofibers were produced by whisker method using a solvent mixture of anisole/chloroform (4:1 vol. %) and spin coated on SiO_2/Si substrates. The concentrations of the solutions were 0.050 wt % (left) and 0.010 wt % (right). Scan size is 5×5 μm. Height scales are 30 nm (image) and 10 nm (cross section).

standard deviations σ_w are listed in Table 2. The w_{av} determined using the CW tip (24−28 nm) was lower than that determined using the Si tip (28−30 nm), probably because the steeper geometry and lower adhesion forces of the CW tip can improve the lateral resolution of the images.[37] The improvement enabled us to obtain a slight increase in w_{av} with an increase in the alkyl chain length, in contrast to constant w_{av} determined using the Si tip. The increase in w_{av} suggests that, in addition to the predominant role played by attractive interactions between the

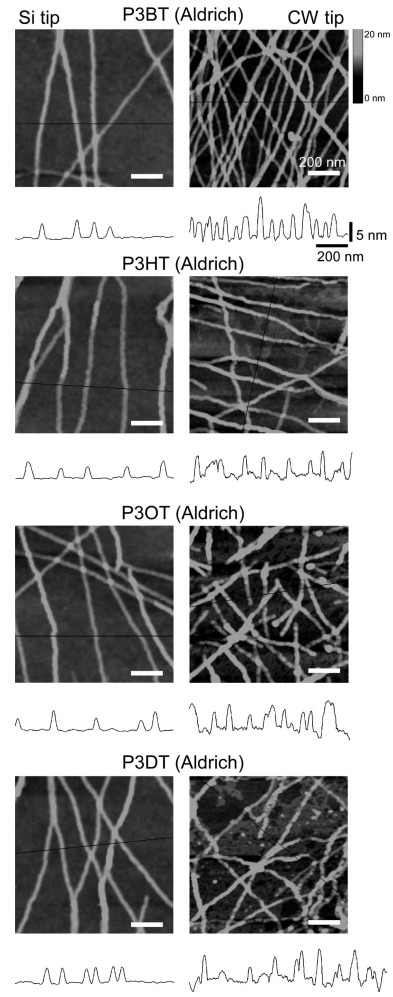

Figure 4. AFM images (upper) and their typical cross sections (lower) of P3AT nanofibers. The nanofibers were produced by whisker method using a solvent mixture of anisole/chloroform (4:1 vol. %) and spin coated on SiO_2/Si substrates. The concentrations of the solutions were 0.010 wt %. Scan size is 1×1 μm. Black solid lines indicate the cross section of the image. Cantilevers having a Si tip (left) and a CW tip (right) were used for the AFM imaging.

Table 2. Results Obtained from Height and Width Histograms of the Nanofibers Determined Using AFM Measurements

		h_{av} (nm)[a]	σ_h (nm)[a]	w_{av} (nm)[b]	σ_w (nm)[b]
Si tip	P3BT (Aldrich)	2.8	0.3	28.2	2.9
		4.1	0.4		
	P3HT (Aldrich)	2.5	0.2	31.3	4.2
		4.2	0.4		
	P3OT (Aldrich)	3.0	0.3	28.7	3.8
		4.8	0.4		
	P3DT (Aldrich)	3.7	0.4	28.3	3.0
		6.0	0.4		
CW tip	P3BT (Aldrich)	3.0	0.8	24.1	4.3
		4.6	0.6		
	P3HT (Aldrich)	3.0	0.1	25.5	4.6
		5.2	1.6		
	P3OT (Aldrich)	4.3	0.6	27.7	3.9
		6.3	1.3		
	P3DT (Aldrich)	4.5	0.8	27.5	4.8
		6.4	0.9		

[a] The height histograms of the nanofibers were fitted by a superposition of two Gaussian curves. [b] The width histograms of the nanofibers were fitted by a single Gaussian curve.

polymer backbones, the alkyl side chain also plays an important role in the stabilization of the nanofiber structure.[24,32,33] This explanation is supported by the result that the polymer chains of RRa-P3HT did not self-assemble into nanofibers because,

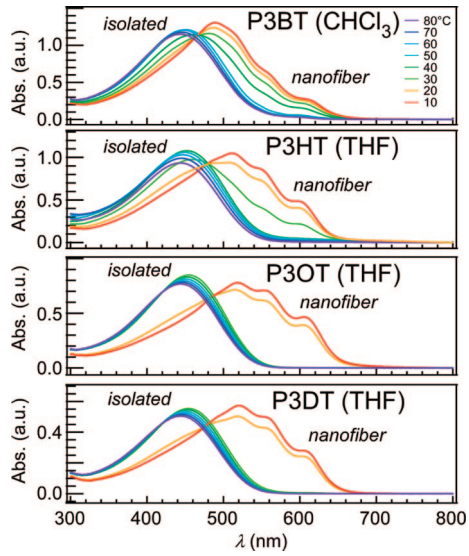

Figure 5. UV−vis absorption spectra of P3AT solutions in anisole (0.025 wt %) during cooling. Soxhlet-extracted P3ATs were used. The thickness of a quartz cell was 1 mm.

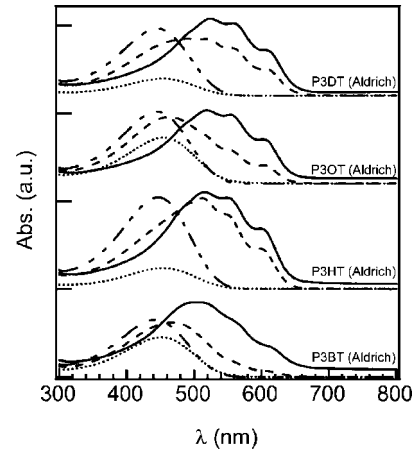

Figure 6. UV−vis absorption spectra of P3AT solutions (0.010 wt %) recorded at 70 °C (dash-dotted line) and at 20 °C (dashed line), P3AT solutions passed through a 0.20-μm PTFE filter at room temperature (dotted line), and thin films of P3AT nanofibers (solid line). A solvent mixture of anisole/chloroform (4:1, vol. %) were used as a solvent.

although an attractive $\pi-\pi^*$ interaction exists between the polymer backbones, a random sequence of alkyl side chains could not stabilize the nanofiber structure.

The careful AFM characterization has determined the height and width of the nanofibers to be 3−4 nm and 24−27 nm, respectively. The nanofiber length of several micrometers presents their high aspect ratio of 100−1000. Similar height and width of P3HT nanofiber have been reported by AFM[17,20,21] and transmission electron microscopy.[17,18] The width of the nanofibers is 5 times larger than their height, indicating that their cross section is anisotropic, not isotropic. The anisotropic cross section of the nanofibers implies the existence of two different origins that determine their height and width, which has been revealed by the following XRD measurement.

UV−Vis Absorption Measurement. Since the solutions of all P3ATs investigated here displayed a drastic color change during nanofiber formation, we investigated in detail the relationship between their UV−vis absorption spectra and nanofiber formation. Figure 5 shows temperature-dependent UV−vis absorption spectra of P3AT solutions. At a higher temperature, the spectra exhibited a single peak at λ_{max} of 445 nm similar to P3AT solutions in chloroform.[8,22a] Because chloroform is a moderately good solvent for P3ATs,[36] this result indicates their complete dissolution in anisole, which is consistent with the result that no spectral change occurred in the solutions after passing through a 0.20-μm PTFE filter at high temperatures (above 70 °C). The absorption spectra recorded at a lower temperature exhibited a decrease in the absorbance at 445 nm and the appearance of vibronic structures at longer wavelengths (500−620 nm) for all the P3ATs investigated. The color change was thermally reversible and was accompanied by large temperature hysteresis (see Supporting Information). Similar spectra have been reported as temperature-dependence of a P3HT solution in 2,5-dimethyltetrahydrofuran[38] and solvatochromism associated with nanofiber formation.[21] Isosbestic points were observed around 480 nm in the absorption spectra recorded in a temperature range of 10−80 °C, suggesting two different states of P3AT in a solution. Although no macroscopic precipitate was observed, the passage through a 0.20-μm PTFE filter left brown or purple solids and caused the resulting filtrate to turn yellow. The absorption spectra of the filtrate showed a drastic decrease in the absorbance at 500−620 nm, leading to a single peak at λ_{max} nearly the same as that of the high-temperature solutions (dotted lines in Figure 6). AFM imaging confirmed that the filtrate did not contain nanofibers. As a result, the absorbance at 500−620 nm was ascribed to the nanofibers and consequently the origin of the two different states was revealed: one state is an isolated polymer chains completely dissolved in a solution and the other state is a polymer aggregate dispersed in a solution, which corresponds to the one-dimensional nanofibrillar structure visualized by AFM. Although a previous study has revealed the appearance of vibronic structures at longer wavelengths was ascribed to microcrystalline aggregates in a solution,[38] the geometry of the aggregates has not been characterized yet. At high temperatures, an isolated P3AT chain has a flexible-coiled conformation, thereby shortening the conjugation length. Heffner et al. have determined the persistent length of P3HT in chloroform to be 2.4 nm,[36] which is much smaller than the width of the nanofibers. λ_{max} slightly shifted to longer wavelength during cooling due to an increase in the conjugation length (see Supporting Information). On the other hand, at near room temperature, P3ATs self-organized into the nanofibers consisting of a stack of polymer backbones. The stacking structure not only provides more extended conformation of the polymer chains but also restricts the rotational motion of the polymer backbones so that it can provide much longer conjugation length than an isolated P3AT and gives an absorbance increase at 500−620 nm.[38] The residual P3ATs in the filtrate were collected by vacuum drying and their molecular weights were determined from SEC measurements. Resulting M_n and M_w/M_n of the P3ATs were as follows: M_n and M_w/M_n of P3BT were, respectively, 6400 and 1.26; P3HT, 8400 and 1.27; P3OT, 11700 and 1.35; P3DT, 13400 and 2.00. These M_n values were much smaller than those of the corresponding starting P3ATs, indicating that the high-molecular-weight fraction of the P3ATs was selectively removed by filtering out the nanofibers. A simple explanation for this is that high-molecular-weight P3ATs, which formed nanofibrillar aggregates that dispersed in a solution, were filtered out, and on the other hand, low-molecular-weight P3ATs, which still be isolated, remained in the filtrate. Surprisingly, the self-organized nanofiber formation showed a stronger preference for the high-molecular-weight P3ATs than the lower-molecular-weight ones and exhibited molecular-weight selection even when the starting P3ATs had a wide molecular-weight distribution (M_w/M_n of 2−4). This explanation was further supported by the following discussion of the nanofiber formation using Soxhlet-extracted P3ATs.

Figure 7 shows absorbance change of P3AT solutions at 600−620 nm during cooling process. P3ATs with shorter alkyl

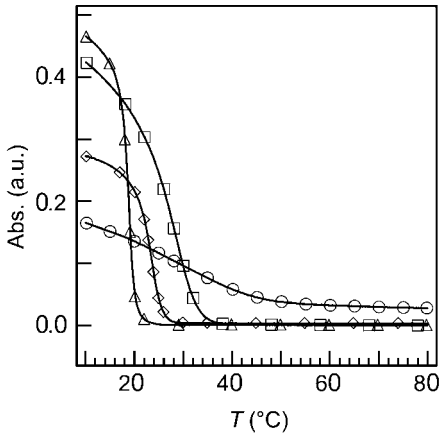

Figure 7. Absorbance change in the peak at 600−620 nm for P3AT solutions in anisole (0.025 wt %) during cooling (25 °C/h). Soxhlet-extracted P3ATs were used: P3BT ($CHCl_3$), circle; P3HT (THF), square; P3OT (THF), triangle; P3DT (THF), diamond symbols. The lines are a guide to the eye.

chains showed a gradual increase in the absorbance at higher temperatures (49 °C for P3BT and 37 °C for P3HT), whereas P3ATs with longer alkyl chains exhibited a rapid increase in the absorbance at lower temperatures (23 °C for P3OT and 28 °C for P3DT). Because the absorbance at 500−620 nm was ascribed to the $\pi-\pi^*$ band of P3AT in the nanofibers, the absorbance change closely relates to nanofiber formation. Here, we can expect the analogy between the gelation in a P3AT/xylene system and the nanofiber formation in a P3AT/anisole system because the formation of fibrillar structures is responsible for both of the systems with slight difference in solvent and concentration. According to the gelation model of the P3AT/xylene system,[32] the nanofiber formation is involved in a two-step process: (1) coil-to-rod conformational transition of a polymer chain and (2) crystallization of rod-like polymer chains into fibrillar aggregates. Because the activation energy of the crystallization of polymer chains is larger than that of their conformational transition for P3HT and slightly smaller for P3DDT,[32c] by assuming that the similar activation energy values are present in our system, crystallization appears to be the rate-determining step for the nanofiber formation of P3ATs having shorter alkyl chains whereas the conformational transition appears to be the rate-determining step for the nanofiber formation of P3ATs having longer alkyl chains. This is consistent with the following explanation of the absorbance change: the slow kinetics of the formation of critical-size nuclei dominates the nanofiber formation accompanying the gradual increase in the absorbance of P3ATs having shorter alkyl chains, whereas slow conformational transition of the polymer chains followed by their rapid crystallization results in the rapid increase in the absorbance of P3ATs having longer alkyl chains.

All the UV−vis absorption spectra of P3AT nanofiber thin films exhibited a maximum at 505−525 nm and two peaks at 550−560 and 600−615 nm (solid lines in Figure 6). Although the thin films showed an absorbance increase at 500−620 nm, their peak wavelengths were almost the same as those of the respective nanofiber solutions. This indicates that the conjugation length of P3AT in the nanofibers dispersed in a solution is comparable to that of P3AT in the nanofiber thin film on the substrate and supports that the nanofibers formed in the solution.

X-ray Diffraction Measurement. Figure 8 shows XRD patterns of P3AT nanofibers. Similar patterns were obtained for both the nanofibers of P3ATs as received from Aldrich and those of Soxhlet-extracted P3ATs. The patterns exhibited two clear peaks, one at a lower diffraction angle of 3−7° and the other at a higher angle of 23°. The XRD spectra, similar to those of the

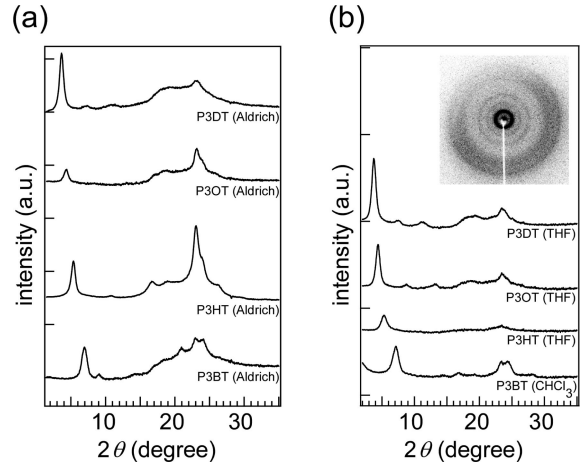

Figure 8. XRD patterns of P3AT nanofibers. Since the nanofibers were randomly oriented, all the nanofibers exhibited ring-like diffraction pattern. (a) Nanofibers were produced from 0.10-wt % solutions in anisole using P3ATs as received from Aldrich and collected by drying in *vacuo*. (b) Nanofibers were produced from 0.050-wt % solutions in a solvent mixture of anisole/chloroform (4:1, vol. %) using Soxhlet-extracted P3ATs and collected by precipitation from methanol. Inset: Two-dimensional XRD pattern of the P3DT nanofiber.

Table 3. Interlayer Distance d and the Size ξ of the Coherent Domains (Crystallite) of the (100) and (020) Peaks Determined by the XRD Pattern

	d_{100} (nm)[a]	ξ_{100} (nm)[a]	d_{020} (nm)[b]	ξ_{020} (nm)[b]
P3BT (Aldrich)	12.7	9.0	3.8	3.5
P3HT (Aldrich)	16.5	10.5	3.8	6.0
P3OT (Aldrich)	20.5	10.5	3.8	6.9
P3DT (Aldrich)	24.1	11.0	3.8	7.3
P3BT ($CHCl_3$)	12.4	7.4	3.7	4.1
P3HT (THF)	16.6	8.3	3.8	3.1
P3OT (THF)	20.1	10.8	3.8	8.4
P3DT (THF)	23.5	10.8	3.8	7.1

[a] The (100) peak were fitted by a Gaussian curve. [b] Since a few peaks overlapped each other at 17−27°, the resulting broad pattern was fitted by a superposition of two or three Gaussian curve.

thin films of P3ATs in previous studies (type-I polymorph in ref 25d),[8b,25,39] suggest that the nanofibers form microcrystalline structures similar to those observed in the thin films of P3ATs. The interlayer distance d and the size ξ of the coherent domains (crystallite) of the diffraction peaks are summarized in Table 3. The peak at 3−7° shifted to lower angles with increasing alkyl chain length, and the corresponding interlayer distance of the (100) diffraction, d_{100}, showed a linear increase as a function of the number of carbon atom in the alkyl side chain. The slope and section of the linear plot were determined to be 1.9 Å and 5.1 Å, respectively. Assuming that a C−C bond length is 1.545 Å and a C−C−C bond angle is 110.5°,[40] twice the molecular length of the alkyl chains on all-trans conformation increases by 2.53 Å per methylene group, indicating that the alkyl side chains on all-trans conformation are tilted at about 40° with respect to the normal direction along the polymer backbone. The section of the linear plot was comparable to the width of a polythiophene backbone.[41] The d_{100} is almost the same value as the summation of twice the molecular length of the alkyl chains on all-trans conformation tilted and the width of a polythiophene backbone, suggesting their minimal interdigitation.[25] In contrast to the lower diffraction peak, the higher diffraction peak was almost constant at 23° independent of the alkyl side chain length, and the interlayer distance corresponding to the (020) diffraction, d_{020}, was determined to be 3.8 Å, which is the stack distance of polythiophene backbones. Analogous to a molecular model proposed for a P3AT thin film,[8b,25,39] a P3AT nanofiber consists of the extended polymer backbones

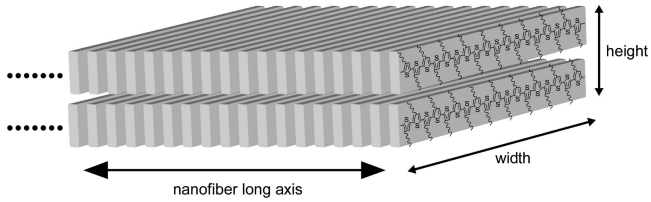

Figure 9. Schematic illustration of a P3AT nanofiber.

stacked along the nanofiber long axis and of laminated layers of the polymer backbones separated by alkyl side chains. A schematic illustration of a possible nanofiber structure is shown in Figure 9. A similar nanofiber model has been proposed in previous studies.[17−20,24] The nanofiber width of 24−27 nm corresponds to 60−70 monomer units as calculated from the 0.39-nm length per a thiophene unit along the extended polymer backbone (*c*-axis) direction. This number of monomer units is smaller than that of as-received P3ATs (except for P3OT), implying the possibility that the nanofiber accompanies folding of P3AT chains. The nanofiber height of 3−4 nm indicates that 2−3 layers of polymer backbones were laminated perpendicular to the long axis of the nanofibers. Strong (100) diffraction peaks corresponding to the alkyl chain direction indicate that the alkyl chain in P3AT nanofibers have a more or less crystalline structure, which plays an important role in the stabilization of the nanofiber structure. Self-organized nanofiber formation was induced by both of the strong $\pi-\pi^*$ interaction between polymer backbones and the crystallization of alkyl side chains. In comparison with a few layers in the height direction, more than 10^4 layers stacked along the nanofiber long axis, as calculated from the d_{020} of 3.8 Å and the nanofiber length of several micrometers. This indicates that the origin of nanofiber formation is highly anisotropic, quasi-one-dimensional crystallization of P3ATs, which is probably caused by larger attractive interaction between polymer backbones than that between alkyl side chains. The ξ_{100} of 7−10 nm corresponds to about twice the height of the nanofibers. This may indicates the slight correlation between nanofibers during solidification. The ξ_{020} of 3−8 nm corresponds to 8−21 stacking layers of P3AT. Because the nanofiber consists of more than 10^4 layers, this result indicates each nanofiber contains many domains of stacking structure, not a single domain. If we assume the domains are separated by a single defect layer, the ratio of the coherent domain is calculated to be 87−95%, which is approximately similar to the regioregularity of the P3AT. This may suggest the regioregularity of the polymer chain determines the size of the coherent domain along the long axis of the nanofiber, which is consistent with the result of P3AT thin films previous reported.[6a] Both the ξ_{100} and ξ_{020} slightly increase with longer side chains, indicating that the alkyl chains enhance the crystallinity of the nanofibers.

Dependence of Nanofiber Formation on Molecular Weight. To clarify the effect of molecular weight, we further examined nanofiber formation of Soxhlet-extracted P3ATs. The results are summarized in Table 4. Whereas the solutions of all P3ATs were orange at high temperatures (above 70 °C), their appearance during cooling was classified into three groups: (1) the solutions that turned brown or purple at 20 °C within 12 h, (2) the solutions that were orange within 12 h and turned brown after 48 h, and (3) the solutions that remained orange after 48 h. The first, second, and third groups respectively correspond to high-, middle-, and low-molecular-weight fraction of P3ATs. The brown and purple solutions yielded nanofibers on a substrate (shown in Figure 10), while the orange solution did not. Because nanofiber formation requires extended rod-like conformation of polymer backbones, the conformational entropy of the polymer

Table 4. Dependence of Nanofiber Formation on the Molecular Weight of P3AT[a]

		hexane		CH_2Cl_2		THF		$CHCl_3$	
		12 h	48 h	12 h	48 h	12 h	48 h	12 h	48 h
P3BT	appearance[b]	or	or	or	or	br	br	pu	pu
	nanofiber[c]	−	−	−	−	+	+	+	+
P3HT	appearance	or	or	or	br	pu	pu		
	nanofiber	−	−	−	+	+	+		
P3OT	appearance	or	or	or	br	pu	pu		
	nanofiber	−	−	−	+	+	+		
P3DT	appearance	or	br	pu	pu	pu	pu		
	nanofiber	−	+	+	+	+	+		

[a] A Soxhlet-extracted P3AT (0.050 wt %) dissolved in a solvent mixture of anisole/chloroform (4:1, vol. %) at 70 °C, and then the solution was cooled to 20 °C at the rate of 25 °C/h and kept at 20 °C for 12 h and 48 h. AFM images confirmed whether nanofibers formed or not. [b] Appearance: or, orange solution; br, brown solution; pu, purple solution. [c] Nanofiber: +, formed; −, did not form.

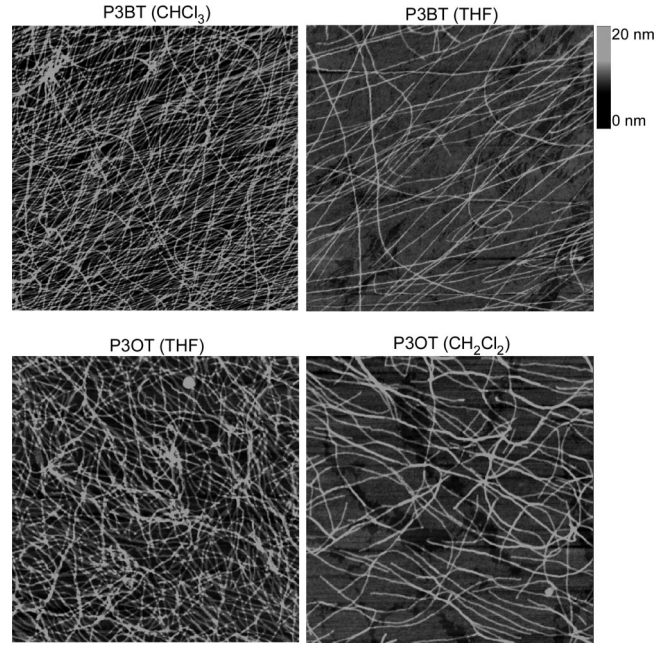

Figure 10. AFM images of P3AT nanofibers. The P3AT nanofibers were produced from a 0.050-wt % solution in a solvent mixture of anisole/chloroform (4:1, vol. %) using the corresponding Soxhlet-extracted P3AT. Scan size is 5 × 5 μm and height scale is 20 nm.

chains decreases significantly on nanofiber formation. The cooperative attractive interactions between polymer backbones and between alkyl side chains for high- and middle-molecular-weight P3ATs, which increase with the length of polymer backbones, seemed to compensate the loss of conformation entropy of the polymer chains and energetically stabilize the nanofiber structure. On the other hand, a weak interaction between short polymer backbones could not stabilize the nanofiber structure. The 60−70 monomer units as calculated from the nanofiber width of as-received P3ATs seem to be a threshold for nanofiber formation. High-molecular-weight P3ATs form nanofibers more rapidly than middle-molecular weight ones, probably due to a lower saturating concentration.

Conductivity Measurements. The carrier transport in a nanofiber network was measured using electrodes whose spacing (36 μm) is much larger than the length of the nanofibers. The spin coating of a 0.050-wt % nanofiber solution produced a nanofiber thin film on an OTS-modified substrate. The P3AT nanofibers, except for P3HT, uniformly distributed between the electrodes and exhibited no aggregates in optical-microscope images; P3HT nanofibers formed several aggregates on the substrate (see Supporting Information). Although the hetero-

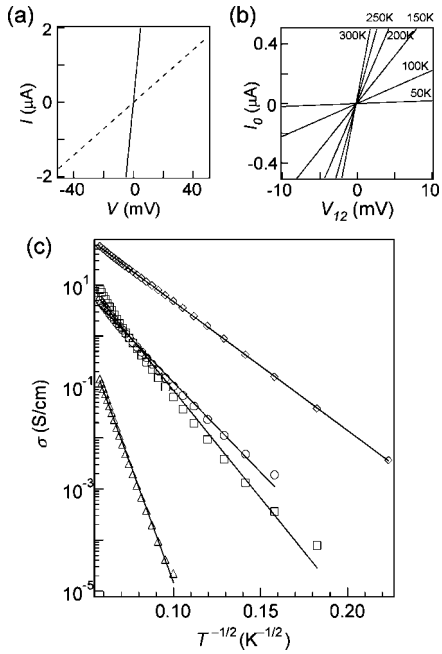

Figure 11. (a) Current−voltage characteristics of P3DT nanofiber network doped with $AuCl_3$ measured by two- (dashed line) and four-probe methods (solid line). (b) Four-probe I_0-V_{12} characteristics of the P3DT nanofiber network at various temperatures. (c) Temperature dependence of the four-probe conductivity σ of P3AT nanofiber networks plotted as a function of $T^{-1/2}$. Open symbols show data points: P3BT (circles), P3HT (squares), P3OT (triangles), and P3DT (diamonds). Solid lines show the fitting lines of a quasi-one-dimensional VRH model given by eq 4.

geneous thickness of the P3HT nanofiber thin films may influence the conductivity analysis, we neglect it for simplicity. AFM images of the thin films show a dense network of nanofibers between the electrodes (see Supporting Information). The surface coverage of the nanofibers was 70−80% mostly independent of the alkyl chain length of P3ATs. Since the contact between an organic semiconductor and a metal electrode is an important issue in the field of organic electronics, two- and four-probe current−voltage characteristics, $I-V$ and I_0-V_{12}, of the nanofiber networks were measured in order to estimate the contact resistance between a P3AT nanofiber and a platinum electrode. As shown in Figure 11a, clear Ohmic behaviors in both of the $I-V$ and I_0-V_{12} characteristics respectively gave two- and four-probe conductance, G_{two} and G_{four}, of the nanofiber networks. The G_{two}, G_{four}, G_{two}/G_{four}, σ_{300K}, and R_c values are summarized in Table 5. The R_c values were on the order of 10^2-10^4 Ω cm. Smaller σ_{300K} on the order of 0.1−10 S/cm gave the G_{two}/G_{four} ratio of 0.4−0.6 whereas larger σ_{300K} on the order of 100 S/cm gave the G_{two}/G_{four} ratio smaller than 0.1. The contact resistance has a crucial influence on two-probe conductivity measurement if the nanofiber has a large conductivity (∼100 S/cm). Work function, surface chemistry and geometry of metal electrodes may affect the contact between the electrodes and the nanofibers. Since higher work function of platinum than gold can result in less injection barrier at the interface,[42] we used platinum for the metal electrode. Typical height and roughness of the platinum electrodes was respectively 10 and 1 nm, which is quite smaller than those of conventional gold electrodes. As far as visualization with AFM, the nanofibers were not distorted at the edge of the electrodes. Nevertheless, the height and roughness of the electrode may have an influence on the contact because the stacking structure of polymer chains in the nanofiber might be slightly deformed at the edge of the electrodes.

The temperature dependences of I_0-V_{12} characteristics for the nanofiber networks were measured at applied voltages ranging from −0.1 to +0.1 V (shown in Figure 11b). Qualitatively similar I_0-V_{12} characteristics were obtained, independent of the alkyl chain length of P3ATs, up to 100 K for P3OT and 40 K for the other P3ATs. Below these temperatures, the current decreased to the background current. Note that even after subjecting the $AuCl_3$-doped nanofibers to these temperature variation measurements the σ_{300K} was nearly the same as that obtained before the measurements. Neither degradation nor dedoping of the doped nanofibers occurred during the conductivity measurements (typically for a few days) due to high stability of the $AuCl_3$-doped nanofibers in contrast to low stability of iodine-doped nanofibers (see Supporting Information). Figure 11c shows the temperature dependence of the four-probe conductivity σ of the nanofiber networks. The σ decreased with temperature. For all the P3ATs, the logarithmic plot of σ as a function of T^{-1}, which explains thermally activated hopping of carriers, could not be fitted by a single linear function. On the other hand, the logarithmic plot of σ as a function of $T^{-1/2}$ was well described by a single linear function. For all the P3ATs, the carrier transport in their $AuCl_3$-doped nanofiber networks could be explained with a quasi-one-dimensional variable-range hopping (VRH) model described by eq 4:[43]

$$\sigma = \sigma_0 \exp\left[-\left(\frac{T_0}{T}\right)^{1/2}\right] \tag{4}$$

$$T_0 = \frac{16}{k_B N(E_F) L_{\parallel} L_{\perp}^{\,2}} \tag{5}$$

where $N(E_F)$ is density of states at Fermi level, $L_{\parallel}$ and $L_{\perp}$ are localization lengths in the directions parallel and perpendicular to polymer backbone, respectively, and T_0 is an estimate of the effective energy barrier between the localized states. The T_0 values obtained from the fitting curve in Figure 11c are listed in Table 5. They show a good correlation with the σ_{300K} values: P3OT nanofibers have the lowest σ_{300K} and the highest T_0; P3DT nanofibers, the highest σ_{300K} and the lowest T_0. A similar correlation has been reported for iodine-doped P3AT thin films.[5] Although the qualitative behavior of the carrier transport was similarly explained by the VRH model for the nanofiber networks of all the P3ATs, the σ_{300K} and the T_0 values were less correlated to the alkyl chain length; the σ_{300K} exhibited over 600-fold variation. Although the origin of this variation is unclear at present, the doping process and/or the crystallinity of nanofiber might be involved because the P3DT nanofiber shows the highest crystallinity and the highest doping ratio (see Supporting Information).

VRH transport results from the carrier localization in nanofiber networks due to a random potential. Nanofiber networks are involved in two carrier-transport processes: carrier transport in a single nanofiber and that between nanofibers. One might expect the possibility that the bridges between the nanofibers disturb the periodicity of the electron density in the nanofiber network, which results in a potential barrier for the carrier transport. In order to examine this possibility by investigating the carrier transport in single nanofibers, we measured the four-probe conductivity of nanofibers using the electrodes whose spacing (250 nm) is much smaller than the length of the nanofibers. Figure 12a shows an AFM image of P3DT nanofibers bridging four-probe platinum electrodes; the number of the nanofibers is about 100. Clear Ohmic behaviors were observed in the I_0-V_{12} characteristics of all the P3AT nanofibers and gave the respective σ_{300K} values as follows: P3BT, 0.56 S/cm; P3HT, 0.81; P3OT, 0.19; and P3DT, 32.6. As compared with the nanofiber networks, the σ_{300K} values of the single nanofibers were slightly smaller. As shown in Figure 12b the temperature

Table 5. Summary of Electrical Characterization of P3AT Nanofiber Networks

	G_{two} (S) [a]	G_{four} (S)[b]	G_{two}/G_{four}	R_c (Ωcm)[c]	σ_{300K} (S/cm)[d]	T_0 (K)[e]
P3BT (Aldrich)	1.14×10^{-5}	2.95×10^{-5}	0.39	9.4×10^{2}	10.7	6.6×10^{3}
P3HT (Aldrich)	2.09×10^{-5}	3.15×10^{-5}	0.66	3.2×10^{2}	9.0	9.4×10^{3}
P3OT (Aldrich)	3.34×10^{-7}	5.79×10^{-7}	0.58	2.5×10^{4}	0.14	4.6×10^{4}
P3DT (Aldrich)	3.54×10^{-5}	4.09×10^{-4}	0.09	5.2×10^{2}	89.0	3.4×10^{3}

[a] G_{two} is the two-probe conductance of a nanofiber netwrok determined from the $I-V$ characteristic at 300K. [b] G_{four} is the four-probe conductance of a nanofiber network determined from the I_0-V_{12} characteristic at 300K. [c] R_c is the contact resistance calculated by eq 3. [d] σ_{300K} is the four-probe conductivity calculated by eq 2. [e] T_0 is an estimate of the effective energy barrier between localized states described by eq 5.

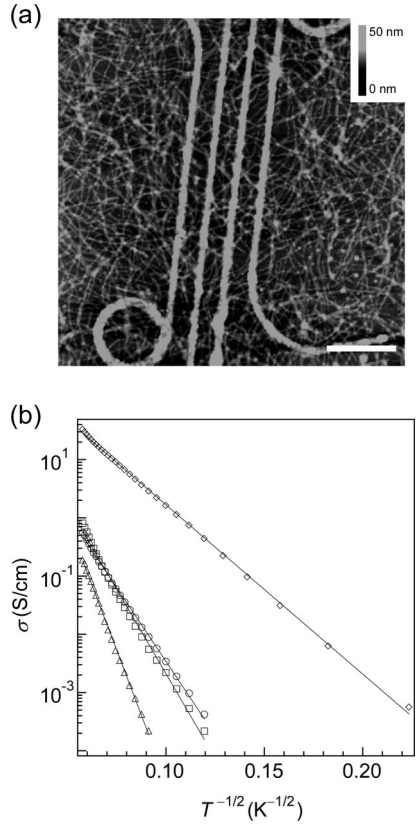

Figure 12. (a) AFM image of P3DT nanofibers bridging four-probe electrodes. The nanofibers were deposited by spin coating of a 0.010 wt % solution. White scale bar is 1 μm. (b) Temperature dependence of four-probe conductivity σ of single nanofibers plotted as a function of $T^{-1/2}$. Open symbols show data points: P3BT, circles; P3HT, squares; P3OT, triangles; P3DT, diamonds. Solid lines show the fitting lines of a quasi-one-dimensional VRH model given by eq 4.

dependence of the conductivity of single nanofibers showed a linear dependence on the logarithmic plot of σ as a function of $T^{-1/2}$, indicating that the carrier transport in single nanofibers could be explained by a quasi-one-dimensional VRH model. The fitting curves in Figure 12b yielded the following T_0 values: P3BT, 1.4×10^4 K; P3HT, 1.8×10^4; P3OT, 4.2×10^4; and P3DT, 4.5×10^3. Surprisingly, the VRH carrier transport in the single nanofibers was not only qualitatively but also quantitatively consistent with that in nanofiber networks; the T_0 values were within 2-fold variation. Since the VRH transport described the carrier transport both in single nanofibers and nanofiber networks, the origin of the random potential that localizes the carriers should be attributed not to the bridges between nanofibers but to some factor involved in a single nanofiber. Unfortunately, there could still be some possibility of the random potential. The localization may occur by the heterogeneous doping of the nanofibers due to a heterogeneous counterion distribution in their vicinity. Randomly distributed defects in the nanofiber can be involved in the random potential because the XRD measurement has revealed that each nanofiber contains many domains of polymer stacking structure. Further, although the carrier transport along polymer backbones is considered to be high due to their regular one-dimensionality of the polymer chains,[1] the carriers migrating along the long axis of the nanofiber results in another possibility of the VRH transport because the long axis of the nanofiber corresponds to the direction of the $\pi-\pi^*$ stacks of polymer backbones.

Conclusion

Effective production of P3AT nanofibers was achieved by means of whisker method using anisole solvent. Attentive AFM characterization using a CW-tip cantilever revealed that the nanofibers had an anisotropic cross section of 3−4 nm height and 24−27 nm width, which slightly increase with the alkyl chain length. UV−vis absorption spectra showed a close correlation between absorbance increase at 500−620 nm and nanofiber formation in a solution, which strongly indicates the extended polymer backbones in the nanofiber. XRD measurements showed that the nanofiber has a microcrystalline structure similar to a thin film of P3AT. The nanofiber structure consists of more than 10^4 parallel stacks of the extended polymer backbones along the nanofiber long axis and of 2−3 laminated layers of the polymer backbones separated by alkyl side chains. Each nanofiber contains many domains of polymer stacking. Nanofiber formation originates from quasi-one-dimensional crystallization of P3ATs, which was induced by both strong $\pi-\pi^*$ interaction between polymer backbones and the crystallization of alkyl side chains. Four-probe conductivities of a nanofiber network and single nanofibers doped with $AuCl_3$ were respectively measured using 36-μm-spacing and 250-nm-spacing electrodes. The temperature dependence of the conductivity showed that the carrier transport of both of the nanofiber networks and the single nanofibers could be explained by a quasi-one-dimensional VRH model. This indicates that the origin of the random potential that localizes the carriers should be attributed not to the bridges between nanofibers but to some factor involved in a single nanofiber.

Acknowledgment. This work was partly supported by a Grant-in-Aid for Scientific Research (KAKENHI) from the Ministry of Education, Culture, Sports, and Science and Technology (MEXT), Japan. S.S. thanks Dr. Toshiyuki Kataoka for his experimental support of X-ray diffraction measurement.

Supporting Information Available: Figures showing the temperature-dependent absorbance for a P3HT solution, temperature-dependent shift of λ_{max} for P3AT solutions, height and width histograms of P3AT nanofibers, optical-microscope images of nanofiber thin films, AFM images of P3AT nanofibers deposited between electrodes, and UV−vis absorption spectra of nanofiber thin films doped with $AuCl_3$ and text giving a brief discussion of chemical doping of P3AT nanofibers. This material is available free of charge via the Internet at http://pubs.acs.org.

References and Notes

(1) (a) Aleshin, A. N.; Lee, H. J.; Park, Y. W.; Akagi, K. *Phys. Rev. Lett.* **2004**, *93*, 196601. (b) Aleshin, A. N.; Lee, H. J.; Jhang, S. H.; Kim, H. S.; Akagi, K.; Park, Y. W. *Phys. Rev. B* **2005**, *72*, 153202. (c) Aleshin, A. N. *Adv. Mater.* **2006**, *18*, 17.

(2) (a) Virji, S.; Huang, J. X.; Kaner, R. B.; Weiller, B. H. *Nano Lett.* **2004**, *4*, 491. (b) Liu, H.; Kameoka, J.; Czaplewski, D. A.; Graighead, H. G. *Nano Lett.* **2004**, *4*, 671. (c) Zhang, X. Y.; MacDiarmid, A. G.; Manohar, S. K. *Chem. Commun. (Cambridge)* **2005**, 5328. (d) Yang, X.; Loos, J.; Veenstra, S. C.; Verhees, W. J. H.; Wienk, M. M.; Kroon, J. M.; Michels, M. A. J.; Janssen, R. A. J. *Nano Lett.* **2005**, *5*, 579. (e) Berson, S.; De Bettignies, R.; Bailly, S.; Guillerez, S. *Adv. Funct. Mater.* **2007**, *17*, 1377. (f) Hu, W. P.; Nakashima, H.; Furukawa, K.; Kashimura, Y.; Ajito, K.; Torimitsu, K. *Appl. Phys. Lett.* **2004**, *85*, 115. (g) Rahman, A.; Sanyal, M. K. *Phys. Rev. B* **2007**, *76*, 045110.

(3) (a) McCullough, R. D.; Ewbank, P. C. In *Handbook of Conducting Polymers*, 2nd ed.; Skotheim, T. A., Elsenbaumer, R. L., Reynolds, J. R., Eds.; Marcel Dekker, Inc.: New York, 1998; Chapter 9, p 225. (b) McCullough, R. D. *Adv. Mater.* **1998**, *10*, 116.

(4) McCullough, R. D.; Nagle, S. T.; Williams, S. P.; Lowe, R. D.; Jayaraman, M.; Anderson, D. L. *J. Am. Chem. Soc.* **1993**, *115*, 4910.

(5) (a) Chen, T.-A.; Rieke, R. D. *Synth. Met.* **1993**, *60*, 175. (b) Menon, R.; Yoon, C. O.; Moses, D.; Heeger, A. J. In *Handbook of Conducting Polymers*, 2nd ed.; Skotheim, T. A., Elsenbaumer, R. L., Reynolds, J. R., Eds.; Marcel Dekker, Inc.: New York, 1998; Chapter 2, p 27.

(6) (a) Sirringhaus, H.; Brown, P. J.; Friend, R. H.; Nielsen, M. M.; Bechgaard, K.; Langeveld-Voss, B. M. W.; Spiering, A. J. H.; Janssen, R. A. J.; Meijer, E. W.; Herwig, P.; de Leeuw, D. M. *Nature* **1999**, *401*, 685. (b) Dhoot, A. S.; Wang, G. M.; Moses, D.; Heeger, A. J. *Phys. Rev. Lett.* **2006**, *96*, 246403.

(7) (a) Jen, K. Y.; Oboodi, R.; Elsenbaumer, R. L. *Synth. Met.* **1986**, *15*, 169. (b) Jen, K.-Y.; Miller, G. G; Elsenbaumer, R. L. *J. Chem. Soc., Chem. Commun* **1986**, 1346. (c) Hotta, S.; Rughooputh, S. D. D. V.; Heeger, A. J.; Wudl, F. *Macromolecules* **1987**, *20*, 212. (d) Nowak, 34, Rughooputh, S. D. D. V, Hotta, S, Heeger, A. J, *Macromolecules*, **1987**, *20*, 965. (e) Sato, M.; Tanaka, S.; Kaeriyama, K. *J. Chem. Soc., Chem. Commun.* **1986**, 873.

(8) (a) McCullough, R. D.; Lowe, R. D.; Jayaraman, M.; Anderson, D. L. *J. Org. Chem.* **1993**, *58*, 904. (b) Chen, T.-A; Wu, X.; Rieke, R. D. *J. Am. Chem. Soc.* **1995**, *117*, 233.

(9) (a) Cai, Z.; Lei, J.; Liang, W.; Menon, V.; Martin, C. R. *Chem. Mater.* **1991**, *3*, 960. (b) Martin, C. R. *Science* **1994**, *266*, 1961. (c) Park, D. H.; Kim, B. H.; Jang, M. K.; Bae, K. Y.; Lee, S. J.; Joo, J. *Synth. Met.* **2005**, *153*, 341. (d) Spange, S. *Angew. Chem., Int. Ed.* **2003**, *42*, 4430. (e) O'Brien, G. A.; Quinn, A. J.; Iacopino, D.; Pauget, N.; Redmond, G. *J. Mater. Chem.* **2006**, *16*, 3237.

(10) (a) Li, D.; Babel, A.; Jenekhe, S. A.; Xia, Y. *Adv. Mater.* **2004**, *16*, 2062. (b) Liu, H.; Reccius, C. H.; Craighead, H. G. *Appl. Phys. Lett.* **2005**, *87*, 253106.

(11) Zhang, X.; MacDiarmid, A. G.; Manohar, S. K. *Chem. Commun. (Cambridge)* **2005**, 5328.

(12) Bjørnholm, T.; Hassenkam, T.; Greve, D. R.; McCullough, R. D.; Jayaraman, M.; Savoy, S. M.; Jones, C. E.; McDevitt, J. T. *Adv. Mater.* **1999**, *11*, 1218.

(13) Maynor, B. W.; Filocamo, S. F.; Grinstaff, M. W.; Liu, J. *J. Am. Chem. Soc.* **2002**, *124*, 522.

(14) Liu, J.; Sheina, E.; Kowalewski, T.; McCullough, R. D. *Angew. Chem.* **2002**, *114*, 339.

(15) (a) Samitsu, S.; Iida, T.; Fujimori, M.; Heike, S.; Hashizume, T.; Shimomura, T.; Ito, K. *Synth. Met.* **2005**, *152*, 497. (b) Samitsu, S.; Shimomura, T.; Ito, K.; Fujimori, M.; Heike, S.; Hashizume, T. *Appl. Phys. Lett.* **2005**, *86*, 233103.

(16) (a) Kline, J.; McGehee, M. D.; Kadnikova, E. N.; Liu, J.; Fréchet, M. J. *Adv. Mater.* **2003**, *15*, 1519. (b) Chang, J.-F.; Sun, B.; Breiby, D. W.; Nielsen, M. M.; Sölling, T. I.; Giles, M.; McCulloch, I.; Sirringhaus, H. *Chem. Mater.* **2004**, *16*, 4772. (c) Yang, H.; Shin, T. J.; Yang, L.; Cho, K.; Ryu, C. Y.; Bao, Z. *Adv. Funct. Mater.* **2005**, *15*, 671. (d) Kline, J.; McGehee, M. D.; Kadnikova, E. N.; Liu, J.; Fréchet, M. J.; Toney, M. F. *Macromolecules* **2005**, *38*, 3312. (e) Zhang, R.; Li, B.; Iovu, M. C.; Jeffries-EL, M.; Sauvé, G.; Cooper, J.; Jia, S.; Tristram-Nagle, S.; Smilgies, D. M.; Lambeth, D. N.; McCllough, R. D.; Kowalewski, T. *J. Am. Chem. Soc.* **2006**, *128*, 3480. (f) Surin, M.; Leclère, Ph; Lazzaroni, R; Yuen, J. D.; Wang, G.; Moses, D.; Heeger, A. J.; Cho, S.; Lee, K. *J. Appl. Phys.* **2006**, *100*, 033712.

(17) Kim, D. H.; Park, Y. D.; Jang, Y.; Kim, S.; Cho, K. *Macromol. Rapid Commun.* **2005**, *26*, 834.

(18) Ihn, K. J.; Moulton, J.; Smith, P. *J. Polym. Sci. Polym. Phys.* **1993**, *31*, 735.

(19) Samitsu, S.; Shimomura, T.; Ito, K. *Thin Solid Films* **2008**, *516*, 2478.

(20) (a) Merlo, J. A.; Frisbie, C. D. *J. Polym. Sci., Polym. Phys* **2003**, *41*, 2674. (b) Merlo, J. A.; Frisbie, C. D. *J. Phys. Chem. B* **2004**, *108*, 19169.

(21) Kiriy, N.; Jähne, E.; Adler, H. J.; Schneider, M.; Kiriy, A.; Gorodyska, G.; Minko, S.; Jehnichen, D.; Simon, P.; Fokin, A. A.; Stamm, M. *Nano Lett.* **2003**, *3*, 707.

(22) (a) Yoshino, K.; Nakajima, S.; Gu, H. B.; Sugimoto, R. *Jpn. J. Appl. Phys* **1987**, *26*, L2046. (b) Yoshino, K.; Love, P.; Onoda, M.; Sugimoto, R. *Jpn. J. Appl. Phys* **1988**, *27*, L2388.

(23) (a) Yoshino, K.; Nakajima, S.; Sugimoto, R. *Jpn, J. Appl. Phys* **1987**, *26*, L1038. (b) Chen, S.-A.; Ni, J. M. *Macromolecules* **1992**, *25*, 6081.

(24) Malik, S.; Nandi, A. K. *J. Polym. Sci. Polym. Phys.* **2002**, *40*, 2073.

(25) (a) Gustafsson, G.; Inganäs, O.; Österholm, H.; Laakso, J. *Polymer* **1991**, *32*, 1574. (b) Tashiro, K.; Ono, K.; Minagawa, Y.; Kobayaehi, K.; Kawai, T.; Yoshino, K. *J. Polym. Sci., Polym. Phys.* **1991**, *29*, 1223. (c) Prosa, T. J.; Winokur, M. J.; Moulton, J.; Smith, P.; Heeger, A. J. *Macromolecules* **1992**, *25*, 4364. (d) Prosa, T. J.; Winokur, M. J.; McCullough, R. D. *Macromolecules* **1996**, *29*, 3654.

(26) (a) Yoshino, K.; Manda, Y.; Sawada, K.; Onoda, M.; Sugimoto, R. *Solid State Commun.* **1989**, *69*, 143. (b) Shin, C.-K.; Lee, H. *Synth. Met.* **2004**, *140*, 177. (c) Ohmori, Y.; Uchida, M.; Muro, K.; Yoshino, K. *Jpn J. Appl. Phys* **1991**, *30*, L1938.

(27) (a) Yoon, C. O.; Reghu, M.; Moses, D.; Heeger, A. J.; Cao, Y.; Chen, T.-A.; Wu, X.; Rieke, R. D. *Synth. Met.* **1995**, *75*, 229. (b) Paloheimo, J.; Stubb, H.; Yli-Lahti, P.; Kuivalainen, P. *Synth. Met.* **1991**, *41*−*43*, 563. (c) Kaneto, K.; Lim, W. Y.; Takashima, W.; Endo, T.; Rikukawa, M. *Jpn. J. Appl. Phys* **2000**, *39*, L872. (d) Babel, A.; Jenekhe, S. A. *Synth. Met.* **2005**, *148*, 169. (e) Park, Y. D.; Kim, D. H.; Jang, Y.; Cho, J. H.; Hwang, M.; Lee, H. S.; Lim, J. A.; Cho, K. *Org. Electron.* **2005**, *7*, 514.

(28) (a) Butt, H.-J.; Guckenberger, R.; Rabe, J. P. *Ultramicroscopy* **1992**, *46*, 375. (b) Hansma, H. G.; Hoh, J. H. *Annu. Rev. Biophys. Biomol. Struct.* **1994**, *23*, 115. (c) Samori, P.; Francke, V.; Müllen, K.; Rabe, J. P. *Chem. Eur. J.* **1999**, *5*, 2312.

(29) (a) Veeco Instruments Inc. Product datasheet of MPP-11100. http://www.veecoprobes.com. (b) NT-MDT Co. Product datasheet of NSC05. http://www.ntmdt-tips.com..

(30) Yang, C.; Orfino, F. P.; Holdcroft, S. *Macromolecules* **1996**, *29*, 6510–6517.

(31) (a) Kato, M.; Ishibashi, M.; Heike, S.; Hashizume, T. *Jpn. J. Appl. Phys., Part 1* **2002**, *41*, 4916. (b) Akai, T.; Abe, T.; Shimomura, T.; Kato, M; Ishibashi, M.; Heike, S.; Choi, B. K.; Hashizume, T.; Ito, K *Jpn. J. Appl. Phys., Part 1* **2003**, *42*, 4764.

(32) (a) Malik, S.; Jana, T.; Nandi, A. K. *Macromolecules* **2001**, *34*, 275. (b) Malik, S.; Nandi, A. K. *J. Phys. Chem. B* **2004**, *108*, 597. (c) Malik, S.; Nandi, A. K. J. *Appl. Polym. Sci.* **2007**, *103*, 2528.

(33) (a) Souto Maior, R. M.; Hinkelmann, K.; Eckert, H.; Wudl, F. *Macromolecules* **1990**, *23*, 1268. (b) Sandstedt, C. A.; Rieke, R. D.; Eckhardt, C. *J. Chem. Mater.* **1995**, *7*, 1057.

(34) Zen, A.; Saphiannikova, M.; Neher, D.; Asawapirom, U.; Scherf, U. *Chem. Mater.* **2005**, *17*, 781.

(35) Grulke, E. A. Solubility Parameter Values. In *Polymer Handbook*, 4th ed.; Brandrup, J., Immergut, E. H., Grulke, E. A., Eds.; Wiley: New York, 1999; Chapter VII, p 675,

(36) Heffner, G. W.; Pearson, D. S. *Macromolecules* **1991**, *24*, 6295.

(37) (a) Zenhausern, F.; Adrian, M.; ten Heggeler-Bordier, B.; Ardizzoni, F.; Descouts, P. *J. Appl. Phys.* **1993**, *73*, 7232. (b) Wong, S. S.; Harper, J. D.; Lansbury, P. T., Jr.; Lieber, C. M. *J. Am. Chem. Soc.* **1998**, *120*, 603.

(38) Rughooputh, S. D. D. V.; Hotta, S.; Heeger, A. J.; Wudl, F. *J. Polym. Sci. Polym. Phys.* **1987**, *25*, 1071.

(39) McCullough, R. D.; Nagle, S.-T.; Williams, S. P.; Lowe, R. D.; Jayaraman, M. *J. Am. Chem. Soc.* **1993**, *115*, 4910.

(40) Abrahamsson, S.; Larsson, G.; Von Sydlow, E. *Acta Crystallogr.* **1960**, *13*, 770.

(41) (a) Thémans, B.; Salaneck, W. R.; Brédas, J. L. *Synth. Met.* **1989**, *28*, C359. (b) Chen, S.-A.; Ni, J.-M. *Macromolecules* **1997**, *25*, 6082.

(42) Hamadani, B. H.; Ding, H.; Gao, Y.; Natelson, D. *Phys. Rev. B* **2005**, *72*, 235302.

(43) (a) Joo, J.; Long, S. M.; Pouget, J. P.; Oh, E. J.; MacDiarmid, A. G.; Epstein, A. *J Phys. Rev. B* **1998**, *57*, 9567. (b) Prigodin, V. N.; Samukhin, A. N.; Epstein, A. J. *Synth. Met.* **2004**, *141*, 155.

MA801128V